Journal of Energy Chemistry 73 (2022) 354–359

Contents lists available at ScienceDirect

Journal of Energy Chemistry

journal homepage: www.elsevier.com/locate/jechem

http://www.journals.elsevier.com/journal-of-energy-chemistry/

Letter

Revealing the dominant factor of domain boundary resistance on bulk conductivity in lanthanum lithium titanates

Xuefeng Zhou [a,b], Cong Gao [b], Dandan Wang [b], Shang Peng [b], Lujun Huang [c], Wenge Yang [b], Wen-Hua Zhang [a,d,*], Xiang Gao [b,*]

[a] Sichuan Research Center of New Materials, Institute of Chemical Materials, China Academy of Engineering Physics, Chengdu 610200, Sichuan, China
[b] Center for High Pressure Science and Technology Advanced Research, Beijing 100094, China
[c] School of Materials Science and Engineering, Harbin Institute of Technology, Harbin 150001, Heilongjiang, China
[d] School of Materials and Energy, Yunnan University, Kunming 650500, Yunnan, China

ARTICLE INFO

Article history:
Received 19 February 2022
Revised 6 June 2022
Accepted 14 June 2022
Available online 18 June 2022

Keywords:
Solid electrolyte
$La_{2/3-x}Li_{3x}TiO_3$
Conductivity
Domain
Domain boundary

ABSTRACT

Perovskite-type lithium lanthanum titanates (LLTO) display a high bulk ionic conductivity and are considered a promising electrolyte for building up to advanced solid-state Li-ion batteries. The LLTO crystals contain a high concentration of intrinsically formed 90°-rotated domain boundaries (DBs) serving as barriers to bulk Li-ion conduction. However, the mechanism of how the DB concentration and DB resistance can compete with each other to determine the bulk conductivity of LLTO is still unknown. Here we report a comprehensive study of LLTO compounds, aimed to unravel the mechanism and hence explore new path(s) for further improving the conductivity of this material. Our results show that both the sintering temperature and chemical composition can affect significantly the domain structures in LLTO. It is found that a decrease in the DB concentration is always accompanied by increased DB resistance due to the increased lattice mismatch at DBs, and vice versa. By unifying the electrochemical impedance spectroscopy and transmission electron microscopy analysis, it is clearly shown that the high DB resistance, instead of DB concentration, acts as the dominant factor governing the bulk conductivity of LLTO. The results thus renew the conventional understanding of the bulk Li-ion conduction in LLTO and shed light on developing novel LLTO electrolyte materials with improved ionic conductivity.

Solid state electrolytes (SSEs) have been intensively studied as potential candidates for replacing highly flammable organic liquid electrolytes in commercial lithium-ion batteries [1–5]. Most of the SSEs, including oxide, sulfide and polymer material systems, are usually subjected to low ionic conductivity, which has been an obstacle to the practical application of the materials [6–8]. The polymer electrolytes, such as the most studied PEO and PVDF-based systems, usually exhibit a low conductivity at room temperature (generally less than 10^{-5} S cm^{-1}) [9–11]. Several sulfide electrolytes, such as $Li_7P_3S_{11}$ and $Li_{10}GeP_2S_{12}$-based electrolytes exhibit a high lithium ionic conductivity up to (1.2–2.5) $\times$ 10^{-2} S cm^{-1} at room temperature, which is comparable with that of organic liquid electrolytes [12–14]. Unfortunately, the sulfides usually have a relatively narrow electrochemical widow and are highly reactive to moisture at room temperature, leading to the release of poisonous hydrogen sulfide gas and hence difficult to produce on a large scale [15,16]. In contrast, many oxide electrolytes have been outstanding for their excellent thermal, and electrochemical stability as well as high ionic conductivity, and hence have attracted considerable attention [17–23].

So far as known, perovskite-type lithium lanthanum titanates, $La_{2/3-x}Li_{3x}TiO_3$ (LLTO, $0 < 3x < 0.5$) exhibit the highest bulk ionic conductivity, i.e. up to the level of 1.0 $\times$ 10^{-3} S cm^{-1} at room temperature [24,25], as compared with the other oxide solid electrolytes. In particular, recent studies found the bulk conductivity of LLTO exceeds even the value of 2 $\times$ 10^{-3} S cm^{-1} by optimizing the materials design and sintering conditions [26,27]. More interestingly, electrochemical impedance spectroscopy (EIS) measurement indicates high energy barrier of E_a = 0.30–0.40 eV for bulk Li-ion mobility in LLTO [24,28,29], while first-principles calculation suggests a low energy barrier of E_a = 0.24–0.31 eV based on averaged crystal structure models for various LLTO compositions [30,31]. Such a discrepancy has been a mystery for understanding the Li-ion mobility in LLTO for quite a long time.

* Corresponding authors.
E-mail addresses: whzhang@caep.cn (W.-H. Zhang), xiang.gao@hpstar.ac.cn (X. Gao).

https://doi.org/10.1016/j.jechem.2022.06.020

Recently, Gao and coworkers reported the origin of such an experiment–theory discrepancy as a result of the formation of mainly considerable 90°-rotation domain boundaries (DBs) in LLTO crystals [32,33]. Based on advanced scanning transmission electron microscopy (STEM), they reported for the first time that the atom structure of various DBs and these DBs are uniformly subjected to interfacial La segregation and significant lattice strain, which would result in much higher interfacial resistance for inter-domain Li-ion migration than that of the inner-domain Li-ion migration. First principles calculation further suggests that in case of the absence of DBs, the bulk conductivity of LLTO ceramics could increase up to three orders of magnitude based on Arrhenius formula, i.e. reaching a new record break-through level of 1 S cm^{-1} for solid-state lithium ionics. However, it would be rather challenging to eliminate the domains and DBs, which are intrinsically formed in LLTO as a result of degraded phase transition during the cooling process from high sintering temperature [34]. In particular, it is still unknown how the DB concentration and DB resistance compete with each other to affect the Li-ion conductivity in LLTO. Furthermore, it was pointed out that both the Li content and synthesis condition can have a significant influence on not only the DB concentration (domain size) and DB resistance [32,35], but also the conductivity of LLTO [36]. To shed light on material design and synthesis, it is highly necessary to explore the dominant factor(s) and their mechanism(s) governing the bulk ionic conductivity of LLTO electrolytes.

In this work, we report a systematic study on the ionic conductivity and domain structure in LLTO crystals fabricated using varied compositions and sintering temperatures. The results reveal for the first time the complex correlations between the synthesis–micro structure–property in LLTO, as well as the critical factor dominating the conductivity of LLTO crystals. The results would pave the way for developing novel solid-state electrolytes with improved performance for large-scale applications in solid-state lithium-ion batteries.

Nine ceramic LLTO samples with three nominal Li content (LLTO1 for $3x$ = 0.16, LLTO2 for $3x$ = 0.33, LLTO3 for $3x$ = 0.40), are fabricated via solid-state reaction method using three different sintering temperatures (1250, 1300 and 1350 °C), as shown in Table S1.

To determine the crystallinity of LLTO ceramic samples, XRD measurement was performed. As shown in Fig. 1(a–c), the main phase was determined as crystalline LLTO, while very weak peaks indicated a very small amount of secondary phase (rutile TiO_2 or/and $La_2Ti_2O_7$) were also discerned in some LLTO samples. It has been reported that these secondary phases are actually ionic insulators, which act as the barriers to intergranular Li-ion conduction [37], i.e., adding up the grain boundary resistance. As indicated by the splitting of characteristic peaks at around 2θ = 47°, it is clear that the Li-poor samples of LLTO1-1250/1300/1350, and Li-rich samples sintered at relatively high temperatures of LLTO2-1300/1350 and LLTO3-1350, show the splitting of the characteristic peaks into (0 0 4)/(2 0 0)/(0 2 0) peaks. While the remains of LLTO2-1250 and LLTO3-1250/1300 display a splitting of the characteristic peaks into (2 0 0)/(0 0 4) peaks. It can be concluded that the Li-poor samples of LLTO1-1250/1300/1350, and Li-rich samples sintered at relatively high temperatures of LLTO2-1300/1350 and LLTO3-1350 exhibit uniformly an orthorhombic crystal symmetry (S.G. Pmmm). While the LLTO2-1250 and LLTO3-1250/1300 exhibit the tetragonal crystal symmetry (S.G. P4/mmm). The splitting of the characteristic peaks in the inset clearly monitors the evolution of crystal structure symmetry with the varied lithium content and sintering temperature. The diffraction peaks at around 2θ = 11.5° for the superstructure correspond to the ordering of cations or vacancies on A-sites. It is obvious that the superstructure peaks gradually become weaker and broader with increasing (decreasing) nominal Li content (sintering temperature). Such a change can be ascribed to the variation of Li content and sintering temperature, which result in the ordering degree of lattice structure and hence the crystal symmetry evolution from orthorhombic to

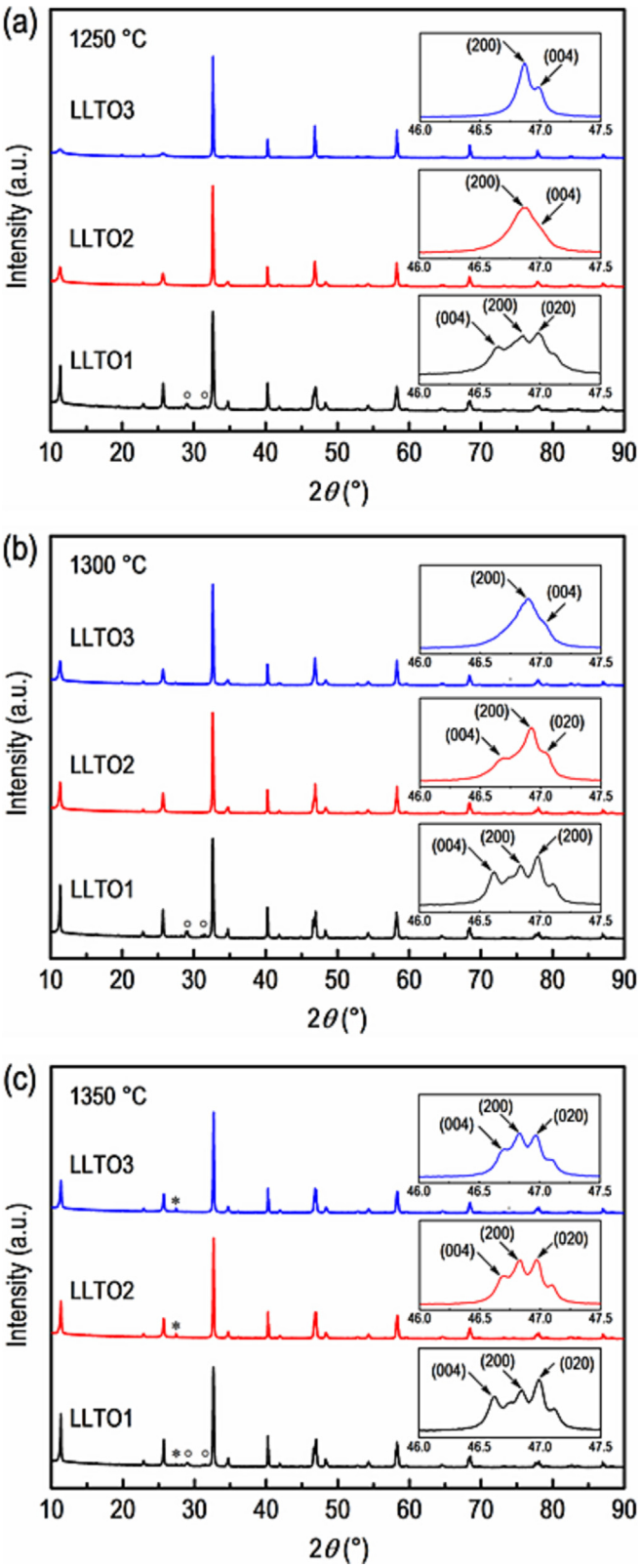

Fig. 1. Powder X-ray diffraction patterns of LLTO ceramic samples sintered at (a) 1250, (b) 1300 and (c) 1350 °C, respectively. The enlarged characteristic diffraction peaks in the 2θ range of 46–47.5° are shown as insets. (*: TiO_2, ○: $La_2Ti_2O_7$.)

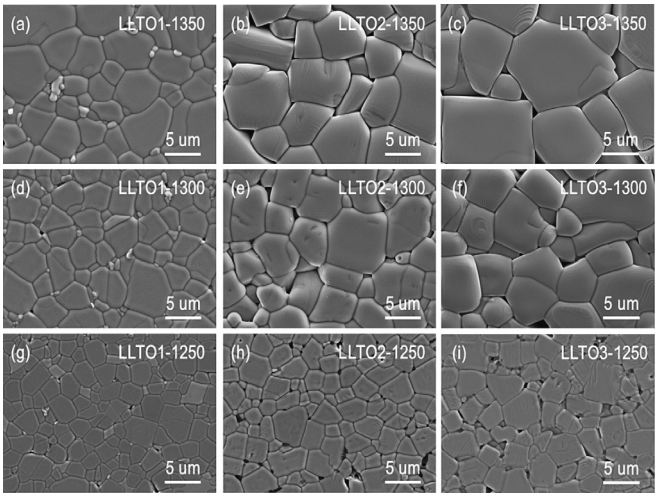

Fig. 2. SEM images showing the surface morphology of LLTO ceramic samples. (a) LLTO1-1350, (b) LLTO2-1350, (c) LLTO3-1350, (d) LLTO1-1300, (e) LLTO2-1300, (f) LLTO3-1300, (g) LLTO1-1250, (h) LLTO2-1250, (i) LLTO3-1250.

tetragonal. These results indicate that either the Li content or the sintering temperature can be utilized to tune the crystal symmetry of LLTO, which is consistent with previous results [25,36]. To understand the structural details of LLTO ceramics, Rietveld refinements were carried out (see Fig. S1 and Table S2 in supporting materials).

As shown in Fig. 2, the SEM observations show clearly that the grain size of LLTO ceramic samples increases with the increasing of lithium content (sintering temperature) at a given sintering temperature (lithium content). The sample density values are shown in Table S3. The relative densities of LLTO samples are all >92%, which are consistent with the SEM observations.

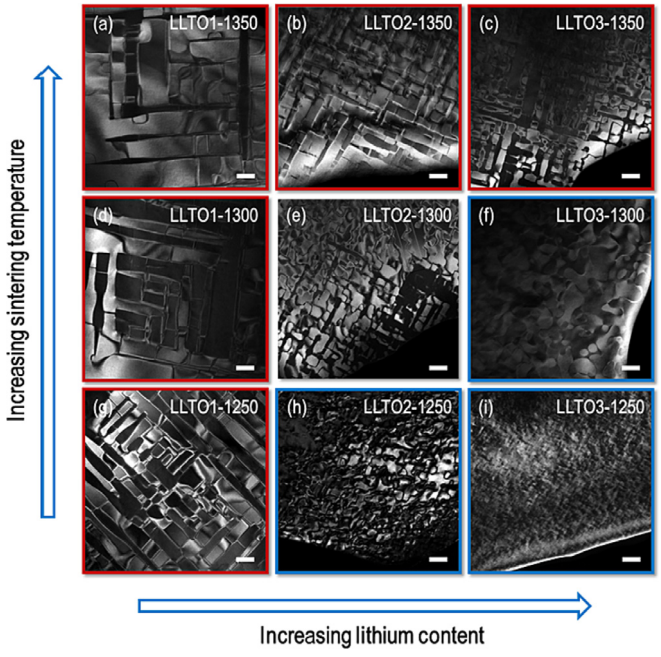

Fig. 3. Two-beam dark-field TEM images showing the typical domain structures in LLTO ceramic samples. (a) LLTO1-1350, (b) LLTO2-1350, (c) LLTO3-1350, (d) LLTO1-1300, (e) LLTO2-1300, (f) LLTO3-1300, (g) LLTO1-1250, (h) LLTO2-1250, (i) LLTO3-1250. The red and blue squares indicate the formation of mainly elongated domains with straight DBs in orthorhombic LLTO crystals (a–d, g) and the formation of smaller mosaic-like domains with curved DBs in tetragonal LLTO crystals (f, h, i), respectively. The LLTO2-1300 exhibits a mixture of the two types of domains. The scale bars in all the figures are 100 nm.

Two-beam dark-field TEM imaging enables direct observation of domain structures in LLTO crystals. Fig. 3 shows the two-beam dark-field TEM images of typical domain structures in LLTO samples. Interestingly, two categories of projected domain patterns are found, depending on the crystal symmetry of LLTO compounds. The orthorhombic LLTO samples (LLTO1-1250/1300/1350, LLTO2-1350, LLTO3-1350) exhibit mainly elongated domains with straight DBs, while the tetragonal LLTO samples (LLTO2-1250, LLTO3-1250, LLTO3-1300) exhibit uniformly much smaller mosaic-like domains with curved DBs, respectively. It is worth noting that, the LLTO2-1300 sample with a medium Li content and sintering temperature shows a mixture of both types of domains. On the other hand, it is clear that the domain size (DB concentration) decreases (increases) with increasing nominal lithium content at a given sintering temperature. Meanwhile, for a given nominal Li content, the DB concentration decreases with increasing sintering temperature. The domain size in relation to experimental Li content of various LLTO samples is roughly estimated from the TEM observation, as shown in Fig. S2.

Fig. S3 shows the experimentally measured Li content is more or less small as compared to its nominal value for LLTO samples. It is well known that such a decrease in lithium content should be caused by lithium loss at high temperatures. In general, a larger ratio of lithium loss is observed to occur in samples having either a higher Li content (at a given sintering temperature) or in samples sintered at higher temperatures (with a given lithium content). While it is rather surprising that the lithium loss can reach up to 39% in LLTO3-1350, which has not been reported so far for this material. Note the detailed measured compositions of LLTO samples are listed in Table S4. The knowledge of real Li content with respect to the designed nominal composition would undoubtedly shed light on a better understanding of the structure-microstructure-property relationship as well as the improved material design of LLTO.

The ionic conductivities of LLTO samples were investigated via electrochemical impedance spectroscopy (EIS) measurement. Fig. 4(a–c) shows Nyquist plots for LLTO samples measured at room temperature, where two well-separated semicircles are observed with a spike. The high-frequency semicircle results from the bulk, and the lower-frequency semicircle corresponds to grain boundary contribution [26]. The impedance data were fitted with the equivalent circuit (see the inset in Fig. 4a–c), where R is the resistance, CPE is the constant phase element and the indices "1", "2" and "3" refer to bulk, grain boundary, and blocking electrode, respectively. All the impedance data were well fitted with such an equivalent circuit by using Zview software, and the bulk conductivity (σ_b), grain boundary conductivity, (σ_{gb}) and total conductivity (σ_{total}) of LLTO samples can be determined according to $\sigma = L/(R \times A)$ (A meaning the area of Pt electrode and L on behalf of the thickness of the ceramic sample) (see Table S5).

Fig. 4(d–f) and Fig. 4(g–i) show typical Arrhenius plots of ionic conductivity in the bulk and at the grain boundary, respectively, for LLTO samples. The conductivity (log σ) shows a linear relationship with the reciprocal of temperature from 0 to 50 °C (see Fig. S4). According to the Arrhenius equation, the activation energy was determined. The activation energies in the bulk of LLTO samples are determined to be in the range of 0.309–0.337 eV, while the activation energies at the grain boundary lie in the range of 0.372–0.401 eV (see Table S5). The grain boundary shows higher activation energy than the bulk, which is in agreement with the previous studies [24,26,27].

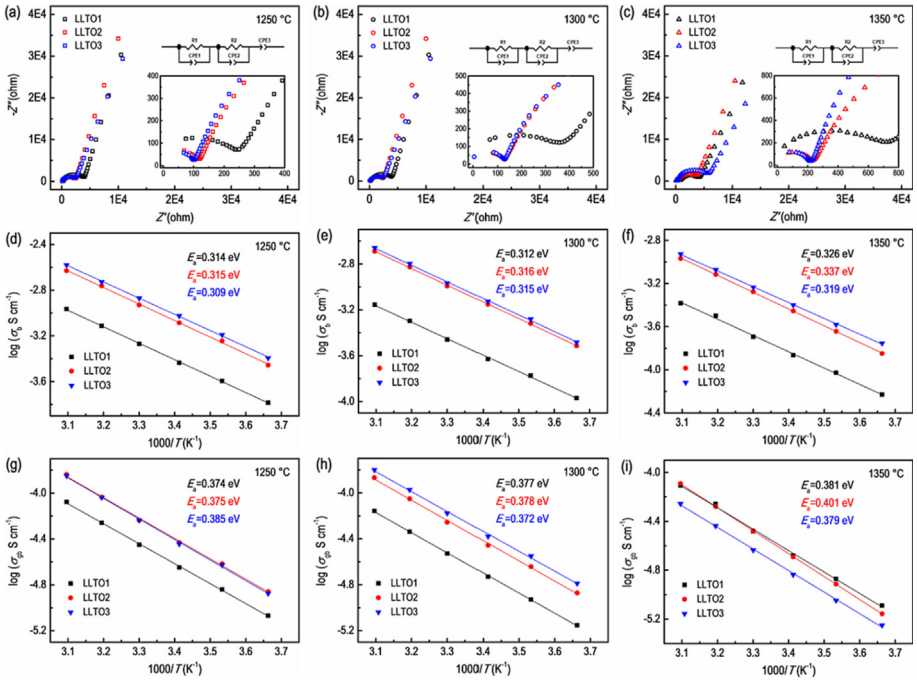

Fig. 4. Electrochemical impedance measurement of LLTO ceramic samples. (a–c) Room-temperature electrochemical impedance spectroscopy (EIS) of LLTO ceramic samples. The corresponding equivalent circuit and the high-frequency semicircle are shown as insets. (d–f) and (g–i) The Arrhenius plots of LLTO ceramic samples in the bulk and at the grain boundary, respectively, where we obtained EIS in the temperature range of 0–50 °C.

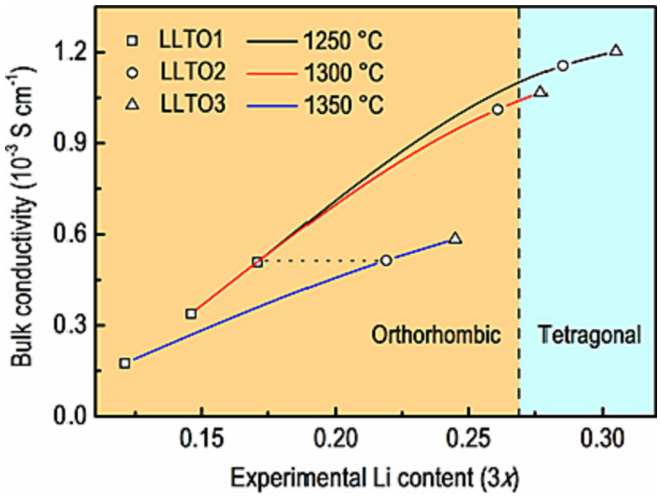

Fig. 5. EIS measured bulk conductivity (σ_b) in relation to the Li content of LLTO ceramic samples. The horizontal dotted line indicates that the LLTO1-1250 and LLTO2-1350 exhibit almost the same σ_b value. The vertical dashed line separates the LLTO ceramic samples having either an orthorhombic (khaki region) or a tetragonal (cyan region) crystal symmetry.

Fig. 5 shows the measured bulk conductivity (σ_b) in relation to the experimental Li content of LLTO ceramic samples. In general, it appears that the σ_b increases with increasing measured Li content ($0 < 3x \leq 0.305$) for a given sintering temperature. It is also shown the tetragonal LLTO samples have a Li-rich composition (LLTO2-1250, LLTO3-1250, LLTO3-1300, $0.277 \leq 3x \leq 0.305$) and show uniformly higher σ_b values as compared to that the orthorhombic LLTO samples which have smaller Li content (LLTO1-1250/1300/1350, LLTO2-1300/1350, LLTO3-1350, $0.121 \leq 3x \leq 0.261$). Based on the results, it seems reasonable to infer that the Li content determines largely the crystal symmetry and hence the bulk ionic conductivity of LLTO, as previously reported [25,36,38,39]. However, such a scenario may not be the true mechanism governing the bulk conductivity of LLTO. For example, it also occurs that the LLTO2-1350 and LLTO1-1250 have almost the same σ_b, nevertheless, the former has a much higher Li content ($3x = 0.219$) than that of the latter ($3x = 0.167$). In particular, there is a large discrepancy of activation energy (E_a) between the experimental data (E_a = 0.30–0.40 eV) from EIS measurement and first-principles calculation results (E_a = 0.24–0.31 eV) based on averaged crystal structure models for bulk Li-ion mobility in LLTO. Note that the E_a in the bulk for LLTO samples of the present study lies in the range of 0.309–0.337 eV, which is consistent with previous results.

Indeed, our previous TEM/STEM study has shown that the direct experimental evidence of the high DB resistance originates from the La segregation and large lattice strain at DBs. The elongated domains in Li-poor orthorhombic LLTO are subjected to severe La segregation and lattice strain at DBs, which impedes significantly Li-ion conduction in the grain interior [32]. While the curved DBs of much smaller mosaic-like domains (high DB concentration) in Li-rich tetragonal LLTO exhibit clearly decreased degree of La segregation and lattice strain at DBs, contributing to decreased DB resistance to Li-ion migration [32]. Based on first principles calculation results and Arrhenius formula, it is illustrated that the large DB resistance should account for the previously reported large discrepancy of E_a between experimental and theoretical results for the bulk ionic conductivity of LLTO, and it is further proposed that the bulk conductivity of LLTO ceramics could increase up to 1000 times higher if the DBs could be removed, i.e. reaching a new record break-through level of 1 S cm^{-1} for solid-state lithium ionics [33]. Based on these results, it is obvious that a lower resistance of the DB structure and a lower DB concentration would be a ben-

efit for achieving a higher bulk conductivity of LLTO. However, based on our observations, the DB structure with a low resistance shows always a high DB concentration, and vice versa. Therefore, it is critical to know how the DB structure and the DB concentration compete with each other to determine the bulk ionic conductivity and thus optimize the property performance of LLTO.

Based on a systematic study, the present work further reveals that both the sintering temperature and composition can be utilized to mediate effectively the domain structure and bulk conductivity of LLTO. By comparing the direct TEM observation of domain structures, it is clearly shown that the tetragonal LLTO samples having a high concentration of curved DBs exhibit uniformly much larger σ_b, as compared to the orthorhombic LLTO samples having a much lower concentration of straight DBs. In particular, the LLTO3-1250 with the highest concentration of curved DBs showed the largest σ_b value ($\sigma_b = 1.2 \times 10^{-3}$ S cm^{-1}), while the LLTO1-1350 with the lowest concentration of straight DBs showed the smallest σ_b value ($\sigma_b = 1.8 \times 10^{-4}$ S cm^{-1}) among all samples. Note that both orthorhombic and tetragonal symmetry does not play a critical factor in the bulk conductivity because of the similar temperature dependence of the bulk conductivity, and slight variation activation energies determined for Li-ion mobility among all LLTO samples [40]. The results indicate that the DB resistance plays a much more dominant role over the DB concentration in determining the bulk conductivity of LLTO. In addition, it is found that the mechanism is also applicable between LLTO samples having the same crystal symmetry of either tetragonal or orthorhombic. The reason for the observed results can be well interpreted based on varied DB resistance in these samples.

It has been reported that either the straight or curved DBs in LLTO is composed mainly of the 90°-rotated DBs (90° DBs), and the high DB resistance originates from the La segregation and large lattice strain caused by lattice mismatch at DBs [32]. In this regard, a larger lattice mismatch would result in a higher DB resistance. There are two types of interface relations at 90° DBs, namely the $(010)_p/(001)_p$ and $(100)_p/(001)_p$, respectively, where "p" refers to the pseudo-cubic perovskite structure of LLTO. Based on an elastic force model, the lattice mismatch (f) for the two types of interface relationships can be estimated from the lattice parameters obtained by XRD, and the results are shown in Table S6. It is found that the varied f values match well with the change of bulk conductivity of LLTO samples as shown above. Therefore, it can be concluded that, an increase in the lattice mismatch at DBs would result in increased DB resistance and hence decreased bulk ionic conductivity of LLTO. It is promising that further development to optimize the conductivity of this electrolyte material can resort to minimizing the lattice mismatch at DBs, while suppressing the DB concentration as much as possible.

In summary, this work presents a systematic study of the crystal structure, domain structure and ionic conductivity of LLTO compounds. It is found that both the sintering temperature and Li content can affect significantly the domain and domain boundary structure as well as bulk ionic conductivity in LLTO. While the real Li content in LLTO could be much smaller than its designed composition as a result of Li loss at high sintering temperatures. Based on an in-depth analysis of the complex structure–microstructure–property relations, our results further verify that the DB structure, which has a high resistance to Li-ion migration as a result of lattice mismatch at DBs, plays a dominant role in determining the bulk ionic conductivity of LLTO. The results reveal for the first time the dominant factor governing the bulk ionic conductivity of LLTO, and shed light on novel directions and routes for further improvements of property performance for this typical solid-state electrolyte material.

Declaration of competing interest

The authors declare that they have no known competing financial interests or personal relationships that could have appeared to influence the work reported in this paper.

Acknowledgments

This work was supported by the National Natural Science Foundation of China (22075003, U2030206).

Appendix A. Supplementary data

Supplementary data to this article can be found online at https://doi.org/10.1016/j.jechem.2022.06.020.

References

[1] M.J. Lee, J. Han, K. Lee, Y.J. Lee, B.G. Kim, K.-N. Jung, B.J. Kim, S.W. Lee, Nature 601 (2022) 217–222.
[2] L. Zhou, T.-T. Zuo, C.Y. Kwok, S.Y. Kim, A. Assoud, Q. Zhang, J. Janek, L.F. Nazar, Nat. Energy 7 (2022) 83–93.
[3] L. Ye, X. Li, Nature 593 (2021) 218–222.
[4] C. Yang, Q. Wu, W. Xie, X. Zhang, A. Brozena, J. Zheng, M.N. Garaga, B.H. Ko, Y. Mao, S. He, Y. Gao, P. Wang, M. Tyagi, F. Jiao, R. Briber, P. Albertus, C. Wang, S. Greenbaum, Y.-Y. Hu, A. Isogai, M. Winter, K. Xu, Y. Qi, L. Hu, Nature 598 (2021) 590–596.
[5] X. Chi, M. Li, J. Di, P. Bai, L. Song, X. Wang, F. Li, S. Liang, J. Xu, J. Yu, Nature 592 (2021) 551–557.
[6] L. Chen, X. Qiu, L.-Z. Fan, J. Energy Chem. 52 (2021) 210–217.
[7] M. Wang, Y. Wu, M. Qiu, X. Li, C. Li, R. Li, J. He, G. Lin, Q. Qian, Z. Wen, X. Li, Z. Wang, Q. Chen, Q. Chen, J. Lee, Y.-W. Mai, Y. Chen, J. Energy Chem. 61 (2021) 253–268.
[8] Y. Yang, H. Zhou, J. Xie, L. Bao, T. Li, J. Lei, J. Wang, J. Energy Chem. 66 (2022) 647–656.
[9] F. Croce, G.B. Appetecchi, L. Persi, B. Scrosati, Nature 394 (1998) 456–458.
[10] Y. Wu, Y. Li, Y. Wang, Q. Liu, Q. Chen, M. Chen, J. Energy Chem. 64 (2022) 62–84.
[11] Y. Zhao, L. Wang, Y. Zhou, Z. Liang, N. Tavajohi, B. Li, T. Li, Adv. Sci. 8 (2021) 2003675.
[12] Y. Seino, T. Ota, K. Takada, A. Hayashi, M. Tatsumisago, Energy Environ. Sci. 7 (2014) 627–631.
[13] N. Kamaya, K. Homma, Y. Yamakawa, M. Hirayama, R. Kanno, M. Yonemura, T. Kamiyama, Y. Kato, S. Hama, K. Kawamoto, A. Mitsui, Nat. Mater. 10 (2011) 682–686.
[14] Y. Kato, S. Hori, T. Saito, K. Suzuki, M. Hirayama, A. Mitsui, M. Yonemura, H. Iba, R. Kanno, Nat. Energy 1 (2016) 16030.
[15] J. Wu, S. Liu, F. Han, X. Yao, C. Wang, Adv. Mater. 33 (2021) 2000751.
[16] Y. Nikodimos, C.-J. Huang, B.W. Taklu, W.-N. Su, B.J. Hwang, Energy Environ. Sci. 15 (2022) 991–1033.
[17] L. Xu, Y. Lu, C.-Z. Zhao, H. Yuan, G.-L. Zhu, L.-P. Hou, Q. Zhang, J.-Q. Huang, Adv. Energy Mater. 11 (2020) 2002360.
[18] Z. Bi, N. Zhao, L. Ma, Z. Fu, F. Xu, C. Wang, X. Guo, Chem. Eng. J. 387 (2020) 124089.
[19] H. Huo, Y. Chen, R. Li, N. Zhao, J. Luo, J.G.P. Silva, R. Mücke, P. Kaghazchi, X. Guo, X. Sun, Energy Environ. Sci. 13 (2020) 127–134.
[20] H. Huo, J. Gao, N. Zhao, D. Zhang, N.G. Holmes, X. Li, Y. Sun, J. Fu, R. Li, X. Guo, X. Sun, Nat. Commun. 12 (2021) 176.
[21] C.-L. Li, B. Zhang, Z.-W. Fu, Thin Solid Films 515 (2006) 1886–1892.
[22] Y. Li, Z. Wang, C. Li, Y. Cao, X. Guo, J. Power Sources 248 (2014) 642–646.
[23] J. Meng, Y. Zhang, X. Zhou, M. Lei, C. Li, Nat. Commun. 11 (2020) 3716.
[24] Y. Inaguma, L. Chen, M. Itoh, T. Nakamura, Solid State Commun. 86 (1993) 689–693.
[25] S. Stramare, V. Thangadurai, W. Weppner, Chem. Mater. 15 (2003) 3974–3990.
[26] H.T.T. Le, R.S. Kalubarme, D.T. Ngo, S.-Y. Jang, K.-N. Jung, K.-H. Shin, C.-J. Park, J. Power Sources 274 (2015) 1188–1199.
[27] S. Sasano, R. Ishikawa, K. Kawahara, T. Kimura, Y.H. Ikuhara, N. Shibata, Y. Ikuhara, Appl. Phys. Lett. 116 (2020) 043901.
[28] Y. Harada, T. Ishigaki, H. Kawai, J. Kuwano, Solid State Ionics 108 (1998) 407–413.
[29] S. Takai, T. Mandai, Y. Kawabata, T. Esaka, Solid State Ionics 176 (2005) 2227–2233.
[30] D.-H. Kim, D.-H. Kim, Y.-C. Jeong, H.-I. Seo, Y.-C. Kim, Ceram. Int. 38 (2012) S467–S470.
[31] M. Catti, Solid State Ionics 183 (2011) 1–6.
[32] X. Gao, C.A.J. Fisher, T. Kimura, Y.H. Ikuhara, A. Kuwabara, H. Moriwake, H. Oki, T. Tojigamori, K. Kohama, Y. Ikuhara, J. Mater. Chem. A 2 (2014) 843–852.

[33] H. Moriwake, X. Gao, A. Kuwabara, C.A.J. Fisher, T. Kimura, Y.H. Ikuhara, K. Kohama, T. Tojigamori, Y. Ikuhara, J. Power Sources 276 (2015) 203–207.
[34] S. Peng, Y. Chen, B. Wang, X. Zhou, H. Yu, J. Wang, W. Yang, X. Gao, Mater. Today, Energy 23 (2022) 100912.
[35] X. Gao, C.A.J. Fisher, T. Kimura, Y.H. Ikuhara, H. Moriwake, A. Kuwabara, H. Oki, T. Tojigamori, R. Huang, Y. Ikuhara, Chem. Mater. 25 (2013) 1607–1614.
[36] H. Geng, J. Lan, A. Mei, Y. Lin, C.-W. Nan, Electrochim. Acta 56 (2011) 3406–3414.
[37] F. Aguesse, V. Roddatis, J. Roqueta, P. García, D. Pergolesi, J. Santiso, J.A. Kilner, Solid State Ionic 272 (2015) 1–8.
[38] Y. Inaguma, L. Chen, M. Itoh, T. Nakamura, Solid State Ionics 70–71 (1994) 196–202.
[39] T. Okumura, T. Ina, Y. Orikasa, H. Arai, Y. Uchimoto, Z. Ogumi, J. Mater. Chem. 21 (2011) 10195.
[40] J. Ibarra, A. Várez, C. León, J. Santamaría, L.M. Torres-Martínez, J. Sanz, Solid State Ionics 134 (2000) 219–228.